

# Seeds Don’t Sink: Even Massive Black Hole “Seeds” Cannot Migrate to Galaxy Centers Efficiently

Lin hao Ma<sup>1,\*</sup>, Philip F. Hopkins<sup>1</sup>, Xiangcheng Ma<sup>2</sup>, Daniel Anglés-Alcázar<sup>3,4</sup>, Claude-André Faucher-Giguère<sup>5</sup> and Luke Zoltan Kelley<sup>5</sup>

<sup>1</sup> TAPIR, Mailcode 350-17, California Institute of Technology, Pasadena, CA 91125, USA

<sup>2</sup> Department of Astronomy and Theoretical Astrophysics Center, University of California Berkeley, Berkeley, CA 94720

<sup>3</sup> Department of Physics, University of Connecticut, 196 Auditorium Road, U-3046, Storrs, CT 06269-3046, USA

<sup>4</sup> Center for Computational Astrophysics, Flatiron Institute, New York, NY 10011, USA

<sup>5</sup> CIERA and Department of Physics & Astronomy, Northwestern University, Evanston, IL 60208, USA

## ABSTRACT

Possible formation scenarios of supermassive black holes (SMBHs) in the early universe include rapid growth from less massive seed black holes (BHs) via super-Eddington accretion or runaway mergers, yet both of these scenarios would require seed BHs to efficiently sink to and be trapped in the galactic center via dynamical friction (DF). This may not be true for their complicated dynamics in clumpy high- $z$  galaxies. In this work we study this “sinking problem” with state-of-the-art high-resolution cosmological simulations, combined with both direct  $N$ -body integration of seed BH trajectories and post-processing of randomly generated test particles with a newly developed DF estimator. We find that seed BHs less massive than  $10^8 M_\odot$  (i.e., all but the already-supermassive seeds) cannot efficiently sink in typical high- $z$  galaxies. We also discuss two possible solutions: forming a huge number of seeds such that one can end up trapped in the galactic center by chance, or seed BHs being embedded in giant structures (e.g. star clusters) with huge effective masses above the mass threshold. We discuss the limitations of both solutions.

**Key words:** black hole physics – galaxies: kinematics and dynamics – galaxies: formation – galaxies: evolution – galaxies: high-redshift – quasars: supermassive black holes

## 1 INTRODUCTION

Supermassive black holes (SMBHs) are of crucial importance in understanding galaxy formation and evolution. Observations of high-redshift quasars have confirmed the existence of SMBHs in the first billion years after the Big Bang (Fan et al. 2001, 2003; Lawrence et al. 2007; Willott et al. 2007; Morganson et al. 2012, see Figure 1 of Inayoshi et al. 2019 for a summary of observations). One of the long standing problems with models of SMBHs regards how they could possibly grow to such an enormous mass in a relatively short time period (Turner 1991). Recent discoveries have found both extremely massive SMBHs in the early universe (e.g. SDSS J010013.02+280225.8 as a  $1.2 \times 10^{10} M_\odot$  SMBH at  $z = 6.3$ , see Wu et al. 2015) and massive SMBHs in the extremely early universe (e.g. ULAS J1342+0928 as a  $7.8 \times 10^8 M_\odot$  SMBH at  $z = 7.54$ , see Bañados et al. 2018). Continued discoveries of SMBHs at higher redshifts and masses naturally makes the problem even more intriguing (Haiman & Loeb 2001).

The existence of such massive black holes (BHs) at such early times poses many unsolved theoretical challenges. The most well-known is the “timescale problem”: if seeds begin life as much less massive BHs, they would have to accrete at  $\sim 100\%$  of the Eddington limit, for  $\gtrsim 100\%$  of the age of the universe to reach their observed masses at  $z > 7$ . But observations at all lower redshifts, and theoretical estimates of the effect of SNe and BH feedback and BH dynamics all argue for much lower duty cycles (see e.g. Johnson & Bromm 2007; Whalen et al. 2008; Alvarez et al. 2009; Milosavljević et al. 2009). An obvious possible solution is to form more massive seeds: it has been proposed that truly primordial gas at high- $z$  could experience inefficient cooling and fragmentation, producing extremely massive Population III stars (Bromm & Larson 2004) which could collapse to BH seeds as large as  $\sim 100 M_\odot$  (e.g. Madau & Rees 2001; Li et al. 2007; Volonteri 2012; Hirano et al. 2014) or even hyper-massive quasi-stars which could leave seeds as large as  $\sim 10^4 - 10^5 M_\odot$  (e.g. Bromm & Loeb 2003; Hosokawa et al. 2012, 2013; Hirano et al. 2017; Inayoshi et al. 2018). Yet several authors

argue that this requires vanishingly improbable conditions (see, e.g. Corbett Moran et al. 2018 and discussions in § 5.2 and § 5.3 from Inayoshi et al. 2019). But even these most-optimistic models only reduce the timescales by a logarithmic factor (as timescales scale as  $1/\log(M_{\text{SMBH}}/M_{\text{seed}})$ ): even in these models, a phase of highly super-Eddington accretion – either resulting from runaway gas capture in incredibly high-gas-density regions (e.g. Madau et al. 2014; Lupi et al. 2016; Pezzulli et al. 2016; Regan et al. 2019), or runaway mergers of massive stars (e.g. Portegies Zwart et al. 2004; Devecchi & Volonteri 2009; Katz et al. 2015; Reinoso et al. 2018) or of other seed BHs (e.g. Davies et al. 2011; Lupi et al. 2014) at the center of a common potential minimum undergoing dynamical relaxation – is likely needed to explain SMBHs at  $z > 7$  (Haiman 2004; Kawashima et al. 2012; Pacucci et al. 2015; Inayoshi et al. 2016; Ryu et al. 2016; Takeo et al. 2019).

However, in the last few years, multiple independent studies (Anglés-Alcázar et al. 2017b; Biernacki et al. 2017; Tremmel et al. 2018; Pfister et al. 2019; Bellovary et al. 2019a; Barausse et al. 2020; Boldrini et al. 2020; Çatmabacak et al. 2020) have pointed out that *all* of these models face a different and potentially even more severe challenge: what we dub the “sinking problem.” In brief: observations and essentially all of these rapid/efficient accretion models require that BHs sink “efficiently” and remain tightly bound to the galaxy center or potential minimum, where densities are on average highest. This may not be possible *dynamically* for even “high” mass seeds in realistic turbulent, clumpy, high-redshift galaxies which undergo frequent dynamical perturbations (from e.g. mergers and “bursty” star formation and stellar feedback) and lack well-defined dynamical centers, especially in the short timescales available. Observationally, SMBHs are seen in the galactic center for most massive quasi-stellar objects (QSOs) (including those at high- $z$  where imaging is possible, e.g. Venemans et al. 2017; Bañados et al. 2019; Decarli et al. 2019; Novak et al. 2019; Wang et al. 2019, and almost *all* massive galaxies comparable to QSO hosts at low redshifts, see e.g. Ferrarese & Merritt 2000; Gebhardt et al. 2000; Tremaine et al. 2002; Graham et al. 2011; Beifiori et al. 2012). But in spatially-resolvable low- $z$  dwarf galaxies where

\* E-mail: lma3@caltech.edu

star formation is known to be “bursty” (Weisz et al. 2014; Sparre et al. 2017; Faucher-Giguère 2018; Velázquez et al. 2020) and there is no well-defined dynamical center (see e.g. Kallivayalil et al. 2013), AGNs are extremely rare and those identified are randomly-scattered in position around the galaxy (Reines et al. 2020; Mezcua & Domínguez Sánchez 2020). As numerical simulations of high- $z$  galaxies have improved in both numerical resolution and incorporating the physics of star formation and stellar feedback in a turbulent, multi-phase ISM, most models have converged toward the prediction that high- $z$  galaxies are extremely clumpy, bursty, chaotic, and dynamically-unrelaxed systems (even more so than most local dwarfs; see e.g. Anglés-Alcázar et al. 2014, 2017b; Muratov et al. 2015; Ma et al. 2018a; Kim et al. 2019; Meng & Gnedin 2020; Kretschmer & Teyssier 2020), in agreement with deep observations with the *Hubble Space Telescope* (HST) (Elmegreen et al. 2007; Overzier et al. 2010; Swinbank et al. 2010). Although there is some evidence for rotation in some hosts as noted by, e.g. Decarli et al. (2018); Venemans et al. (2019), they usually exhibit very large dispersion with  $\sigma \sim v$ , consistent with the simulations analyzed in Ma et al. (2017), which does not challenge the conclusion. But in almost all models for rapid BH growth at near-Eddington or super-Eddington rates at high- $z$ , the most optimistic assumption possible is usually made: namely that the BH remains “anchored” to the local potential minimum at the center of some well-ordered galaxy (e.g. Li et al. 2007). To accrete gas, the BH must first capture it from the surroundings, and dimensional estimates for the “capture rate” drop highly super-linearly and extremely rapidly if the BH or background medium are moving relative to one another and/or if the BH lies outside of the galactic density maximum (Hoyle & Lyttleton 1939). Models like runaway stellar mergers or BH-BH seed mergers for rapid growth fundamentally *depend* on the idea that both the “main seed” BH and all other stars/seeds are anchored to and sinking rapidly towards a common dynamical center (Portegies Zwart & McMillan 2002; Gürkan et al. 2004; Shi et al. 2020; González et al. 2020).

Historically, the “sinking” of BH seeds in high- $z$  galaxies has largely been studied by assuming (1) seeds form at the centers of their proto-galaxies (rather than where stars form or at local density maxima), (2) galaxies are smooth objects with well-defined dynamical centers and centrally-peaked density profiles (i.e. bulge+disk or isothermal sphere models, rather than messy, non-relaxed systems), and (3) that BH and merging galaxy orbits decay according to dynamical friction (DF), which is a statistical accumulative effect caused by successive two-body gravity encounters, effectively acting like a “drag force” proportional to the BH/merging galaxy mass, in which the traditional Chandrasekhar (1943) (C43) DF formula (assuming a homogeneous, infinite, idealized background medium) is applied. In this paper, we therefore revisit the “sinking” and “retention” problems for seed BHs in early galaxies. We use high-resolution cosmological simulations which include the crucial physics described above, combined with both direct (“live”)  $N$ -body integration of seed BH trajectories and semi-analytic orbit integration in post processing, to follow a wide range of possible BH seed populations with different formation properties and locations. In post processing, we apply a modified DF estimator developed in a companion paper (Ma et al. in prep.), which is more flexible, accurate, and computationally efficient. In § 2 we describe our numerical simulations and the semi-analytic post-processing method.

The plan of this paper is as follows: in § 3 we present the results from simulations and semi-analytical integration of sample orbits, and show that seed BHs are generally not able to sink efficiently or be retained even at high seed masses. In § 4, we discuss possible solutions to this problem, but also use our simulations to highlight

how these solutions encounter still other problems. We summarize in § 5.

Throughout, we assume a standard flat  $\Lambda$ CDM cosmology with  $\Omega_m = 0.31$ ,  $\Omega_\Lambda = 1 - \Omega_m$ ,  $\Omega_b = 0.046$ , and  $H_0 = 68 \text{ km s}^{-1} \text{ Mpc}^{-1}$  (e.g. Planck Collaboration et al. 2020).

## 2 METHODS

### 2.1 Direct Simulations

#### 2.1.1 Simulation Details

The simulations we study are re-simulations of the high-redshift ( $z > 5$ ) galaxies presented in Ma et al. (2018a,b, 2019) based on the Feedback In Realistic Environments (FIRE; Hopkins et al. 2014, 2018) project<sup>1</sup>. Specifically, we re-simulate the cosmological zoom-in simulations centered around the galaxies “z9m12a” and “z5m12b”. Each of these represents a galaxy which has reached a halo mass  $\gtrsim 10^{12} M_\odot$ , a stellar mass  $> 10^{10} M_\odot$ , and a star formation rate  $\gtrsim 150 M_\odot \text{ yr}^{-1}$  by redshifts  $z \sim 9$  and 5, respectively. As discussed in Ma et al. (2019), these are chosen to be plausible analogues to the observed hosts of the highest-redshift, brightest QSOs. We note that while there are many other well-resolved galaxies in each cosmological zoom-in volume, we follow the most massive galaxy as it is the best candidate for a QSO host (but our conclusions about failure of BHs to “sink” are even stronger in lower-mass galaxies).

The simulations are run with an identical version of the GIZMO<sup>2</sup> code (Hopkins 2015) to their original versions in Ma et al. (2018b). We use the mesh-less finite-mass (MFM) mode for solving hydrodynamic equations, with the identical FIRE-2 implementation of star formation and stellar feedback. The detailed baryonic physics included are all described extensively in Hopkins et al. (2018), but briefly summarized here. Gas cooling includes a variety of processes (molecular, atomic, fine structure, recombination, dust, free-free, Compton, etc.) accounting for 11 separately tracked species (H, He, C, N, O, Ne, Mg, Si, S, Ca, and Fe), following the meta-galactic UV background from Faucher-Giguère et al. (2009) with self-shielding. Stars are formed on the free-fall time from gas which is locally self-gravitating, molecular/self-shielded, denser than  $n > 1000 \text{ cm}^{-3}$ , and Jeans-unstable following Hopkins et al. (2013). Each star particle, once-formed, represents an IMF-sampled population of known mass, age and metallicity, and we explicitly account for stellar mass-loss (from OB and AGB outflows), core-collapse and Ia supernovae, and radiative feedback (in the forms of photo-ionization and photo-electric heating, and single and multiple-scattering radiation pressure), with rates tabulated from standard stellar evolution models (Leitherer et al. 1999).

The only difference between our simulations and those in Ma et al. (2018b) is that we re-run them including a “live” model for the formation of a broad spectrum of BH seeds, which are allowed to follow the full  $N$ -body dynamics. We emphasize that we do not artificially “force” BHs to follow the potential minimum or decay their orbits via any prescriptions of subgrid DF, as in some cosmological simulations (e.g. Springel et al. 2005; Hopkins et al. 2005, 2006, 2008; Sijacki et al. 2015; Anglés-Alcázar et al. 2017a).

We form BH seeds as follows: whenever gas meets all the star formation criteria above and is about to be transformed into a star particle, it is assigned a probability of instead becoming a BH seed. The probability is weighted so that BH seeds form preferentially at the lowest metallicities and highest surface densities/gravitational acceleration scales: specifically we adopt  $p \propto$

<sup>1</sup> See the FIRE project website: <http://fire.northwestern.edu>

<sup>2</sup> A public version of GIZMO is available at <http://www.tapir.caltech.edu/~phopkins/Site/GIZMO.html>

$\exp(-Z/0.01 Z_\odot)[1 - \exp(-\Sigma/\Sigma_0)]$  where  $\Sigma \sim M/R^2$  is integrated to infinity with the Sobolev estimator from Hopkins et al. (2018) and  $\Sigma_0 = 1 \text{ g cm}^{-2}$  is motivated by simulations of bound star cluster formation (Grudić et al. 2018). The normalization is chosen to form the maximum number of seeds before they begin to represent an appreciable fraction of the total galaxy mass and therefore perturb the dynamics. If the particle is selected to become a BH seed, then we draw a BH seed mass uniformly in  $\log M$  from  $M = 10^3 - 10^7 M_\odot$ .

Because we wish to *only* study the dynamics of BH seeds, we ignore BH accretion or feedback. These will be studied in future work.

### 2.1.2 Resolution and Treatments of (Un)Resolved DF

Our “default” simulations have an approximately constant baryonic mass resolution of  $\Delta m_i \sim 7000 M_\odot$ . This is sufficient to explicitly resolve N-body dynamical friction and other effects on the more massive seeds ( $\gtrsim 10^5 M_\odot$ ) we simulate: depending on the details of the gravity scheme, one generally achieves this for seed masses  $M \gtrsim (10 - 100) \Delta m_i$ .<sup>3</sup> To assess the effects of resolution on the dynamics of lower-mass BH seeds, we briefly re-simulate one of our galaxies after applying a super-Lagrangian (AMR-like) refinement step (e.g. Angles-Alcazar et al. 2020), to run with  $800 M_\odot$  baryonic resolution, and measure whether there is any significant difference in the “sinking rate” of seeds at any BH mass after 100 Myr. We find no measureable difference. There is a simple reason why the detailed numerical accuracy of the DF forces on such low mass seeds has little effect: the actual DF time for low-mass seeds (with e.g.  $M \ll 10^5 M_\odot$ ) is far longer than the Hubble time at these (high) redshifts, so DF plays an essentially negligible role in their dynamics on a *galactic* scale.

## 2.2 Semi-Analytic Orbital Evolution

Both as a check of our direct numerical simulations, and a way to gain analytic insight and explore even larger parameter spaces prohibited by the resolution and computational expense of our simulations, it is useful to have a semi-analytic analysis for the dynamics of BH seeds. In post-processing, we can create an arbitrary sample of BH seeds at any desired time, and evolve them in time-independent potentials taken directly from the numerical simulations, allowing us to map the dynamics in detail.

To do so, we re-calculate the trajectories of a huge number of BH “test particles,” taking background potentials from the simulations and adding an analytic DF force explicitly in post-processing, during which we apply a newly developed DF estimator that is discussed in a companion paper (Ma et al. in prep.). We approximate the N-body dynamics of a seed of mass  $M$  with an acceleration  $\mathbf{a}_M = \mathbf{a}_{\text{ext}} + \mathbf{a}_{\text{df}}$ , where  $\mathbf{a}_{\text{ext}}$  is the “normal” external gravitational acceleration on a test particle (computed identically to how the forces

are computed in-code, for the adaptively force-softened potential from all N-body particles in the simulation). Then  $\mathbf{a}_{\text{df}}$  is the “DF force” – the next-order (non-linear) term which represents the drag force arising from deflection of bodies by  $M$ . Specifically, we adopt the following expressions which can be *directly* computed from the simulation data (either on the fly or in post-processing):

$$\begin{aligned}
 \mathbf{a}_{\text{ext}} &= - \sum_i \left( S_i(r_i) \frac{G \Delta m_i}{r_i^2} \right) \hat{\mathbf{r}}_i \\
 \mathbf{a}_{\text{df}} &= \sum_i \left( \frac{\alpha_i b_i}{(1 + \alpha_i^2) r_i} \right) \left( S_i(r_i) \frac{G \Delta m_i}{r_i^2} \right) \hat{\mathbf{v}}_i
 \end{aligned} \tag{1}$$

Here  $\mathbf{a}_{\text{ext}}$  and  $\mathbf{a}_{\text{df}}$  are defined as a sum over all N-body particles  $i$ , with N-body masses  $\Delta m_i$ , relative position  $\mathbf{r}_i \equiv \mathbf{x}_i - \mathbf{x}_M$ , relative velocity  $\mathbf{V}_i \equiv \mathbf{v}_i - \mathbf{v}_M$ ,  $v \equiv |\mathbf{v}|$  and  $\hat{\mathbf{v}} = \mathbf{v}/v$ , with  $G$  the gravitational constant,  $\alpha_i \equiv b_i V_i^2 / GM$  dimensionlessly parameterizing encounter strength, and  $b_i \equiv r_i |\hat{\mathbf{r}}_i - (\hat{\mathbf{r}}_i \cdot \hat{\mathbf{V}}_i) \hat{\mathbf{V}}_i|$  the impact parameter.  $S_i(r_i)$  is the usual dimensionless force-softening kernel to prevent numerical divergences, defined as

$$S_i(r_i) = \begin{cases} \frac{32}{3} q_i^3 - \frac{192}{5} q_i^5 + 32 q_i^6 & 0 \leq q_i < \frac{1}{2} \\ -\frac{1}{15} + \frac{64}{3} q_i^3 - 48 q_i^4 + \frac{192}{5} q_i^5 - \frac{32}{3} q_i^6 & \frac{1}{2} \leq q_i < 1 \\ 1 & q_i \geq 1 \end{cases} \tag{2}$$

We refer interested readers in our expression for  $\mathbf{a}_{\text{df}}$  to the companion paper (Ma et al. in prep.). But briefly, our expression reproduces exactly the classical Chandrasekhar (1943) (C43) expression  $\mathbf{a}_{\text{df}}^{\text{C43}} = 4\pi G^2 M \rho \ln(\Lambda) V^{-2} [\text{erf}(V/\sqrt{2}\sigma) - (2/\pi)^{1/2} (V/\sigma) \exp(-V^2/2\sigma^2)] \hat{\mathbf{V}}$  in cases consistent with the assumptions of C43, i.e. when the background distribution function is spatially homogeneous (constant density and velocity), time-invariant, Maxwellian, and single-component. But it allows more naturally for cases which violate these conditions. Our expression also removes the ambiguity of the C43 expression in estimating a number of ill-defined continuum quantities, when applied to discrete simulation N-body data (e.g. how and on what scales to evaluate  $\rho$ ,  $\sigma$ ,  $V$ ; what value of  $\Lambda$  to use). Usually,  $\alpha_i \gg 1$  such that  $\mathbf{a}_{\text{df}} \propto \sum \alpha_i^{-1} \propto M$ , which means as expected that the DF acceleration is the largest for the most massive BHs, and potentially negligible for small BHs.

## 3 RESULTS

### 3.1 Direct Simulations

Here we present the results from direct simulations, focusing on the clustering behaviour of BH particles. In Figure 1 we show a projected image of the galaxy “z9m12a” at redshift  $z = 10.4$ , as a typical high redshift snapshot in our simulations. The left panel shows the total non-BH mass (i.e., including dark matter, gas, and stars) density distribution, with the galactic center located at the origin. The image shows the extremely clumpy appearance of typical high- $z$  galaxies, with multiple local density maxima near the galactic center, consistent with both other simulations and observations. In the right panel, we over-plot the positions of BH particles near the galactic center. The color labels their masses, ranging from  $10^3 - 10^7 M_\odot$ , which cover a wide range of seed BH masses from different formation scenarios. There is no significant position dependence upon mass for BH particles in the galaxy, with some mild clustering near the galactic center. No significant mass dependence is observed.

To analyse the sinking problem of seed BHs, we show the magnitudes of galacto-centric distance  $\mathbf{r}$  and velocity  $\mathbf{v}$  of BH particles selected from 9 different snapshots in Figure 2. Specifically, the BH particles are selected from snapshots in “z5m12b” at  $z = 9.0, 7.7, 7.0, 5.9$  and  $5.0$ , and snapshots from “z9m12a” at

<sup>3</sup> We enable the additional improvements to the gravitational timestep criteria, tidal force treatment, tree-opening, and integration accuracy detailed in Guszejnov et al. (2020); Grudić & Hopkins (2020) where they were developed for simulations of star formation which require accurate evolution of stellar binaries and multiples, and set the force softening of the BH seeds to a very small value ( $10^{-3}$  pc) to represent real sink particles while using adaptive force softening for all other types to represent a smooth background. Detailed studies have shown that using adaptive softening as we do to ensure a smooth background force and with the more strict timestep and integration accuracy criteria used here, DF-like forces can be accurately captured for BHs with masses  $\gtrsim 10$  times the background particle mass, while with less accurate integration often used in cosmological simulations which do not intend to resolve few-body effects, the pre-factor is more like  $\sim 100$  (van den Bosch et al. 1999; Colpi et al. 2007; Boylan-Kolchin et al. 2008; Hopkins et al. 2018; Pfister et al. 2019; Barausse et al. 2020; Boldrini et al. 2020).

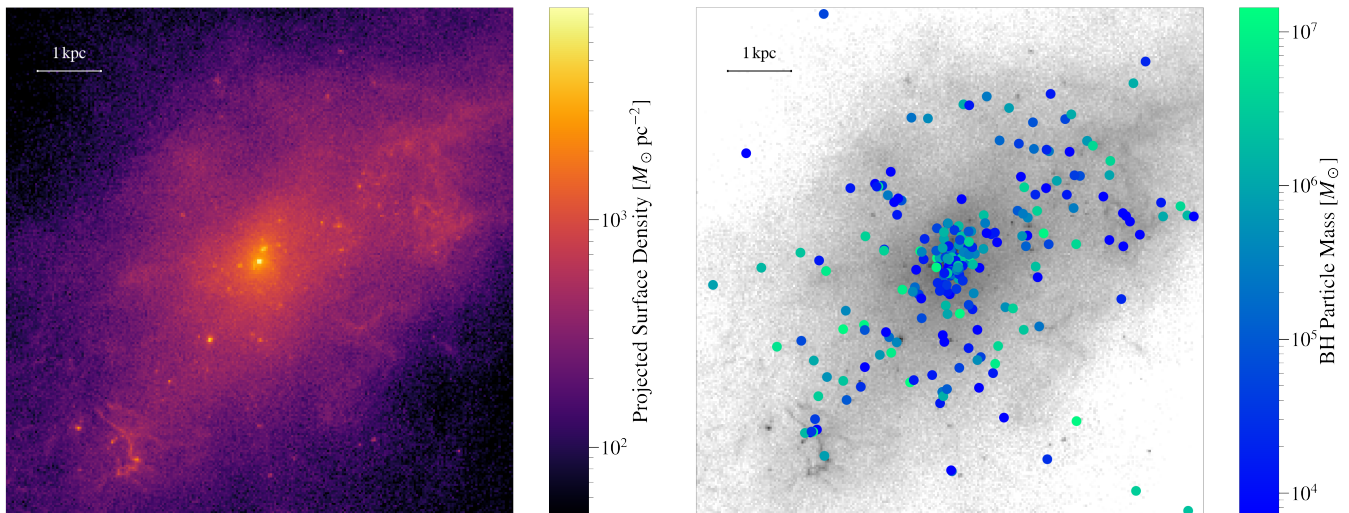


**Figure 1.** **Left:** Projected total non-BH mass (including dark matter, gas, and stars) density distribution of one of our simulations (“z9m12a”) at redshift  $z = 10.4$ , as a typical simulation snapshot we analyze. The image shows the clumpy structure of high redshift galaxies. **Right:** The BH particles in this simulation at this particular snapshot, ranging from  $10^3 - 10^7 M_\odot$ , covering a wide range of possible masses from different seed BH formation scenarios. BHs appear mostly randomly distributed in the galaxy, but with enhanced clustering near the galactic center. However we do not see significant seed-BH mass dependence, and the apparent galactic-center clustering simply reflects the overall concentration of mass (the galaxy effective radius here is  $\sim$  kpc).

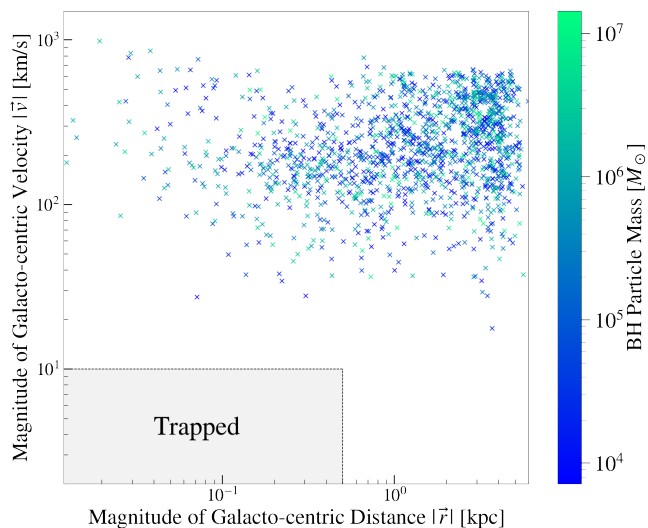


**Figure 2.** The magnitudes of velocities and galacto-centric distances of simulated BH particles for a general selection of snapshots in our simulations. We define a BH particle being trapped and efficiently sinking if it is located within  $< 0.5$  kpc from the galactic center with a speed less than  $10 \text{ km s}^{-1}$  (shaded area). The colors label the mass of each BH particle. From our simulations there are no BH particles trapped in this manner, nor any significant dependence on their masses of their positions and velocities.

$z = 10.9, 10.4, 9.9$  and  $9.5$ . Although snapshots at later redshifts contain BH particles that are already present at earlier redshifts in the same galaxy, the different snapshots are well separated in time such that the positions and velocities of these BH particles can be considered to be statistically independent. If a BH particle is located within  $0.5$  kpc from the galactic center with a (relative) velocity less than  $10 \text{ km/s}$  (Figure 2 shaded area), we consider it to have “efficiently” undergone sinking and trapping in the galactic center. Figure 2 suggests that none of our BH particles in the mass range of  $10^3 - 10^7 M_\odot$  has achieved this at the redshift they are observed. There is also no clear dependence of BH positions and velocities on their masses, indicating their dynamics is basically independent

of their masses if BH masses are below  $10^7 M_\odot$ , i.e. the dynamics is dominated by the mass-independent external gravity, while the mass-dependent dynamical friction plays a negligible role.

### 3.2 Semi-Analytic Orbital Evolution

Here we present the results from semi-analytic post processing, with our new dynamical friction estimator, to cover a wider range of BH masses. Specifically, we select snapshots from “z5m12b” at  $z = 5.0, 7.0, 9.0$  and “z9m12a” at  $z = 9.5$ . In each snapshot, we place 100 test particles to integrate their dynamics, whose initial parameters are generated in the following way: the masses are randomly selected from  $100 - 10^{10} M_\odot$  (uniformly sampling log of mass), while the initial positions and velocities are chosen randomly from star particles in the corresponding snapshot, which is physically motivated since we would expect seed BHs are mostly born in similar locations to star formation. In post processing, we ignore the dynamics of background particles, i.e. we apply a time-independent gravity potential, as we would expect the static background to represent random sample of typical chaotic high- $z$  galaxies, not an accurate reflection of some certain galaxy. The assumption of a static but realistically clumpy mass distribution allows us to gain insight into the effects of spatial inhomogeneities in the gravitational potential expected in typical, chaotic high- $z$  galaxies. However, the orbits that we calculate in this way are not necessarily fully realistic since they neglect the time dependence of the potential. We note, though, that time dependence of the potential seems unlikely to accelerate sinking relative to a static-potential calculation; if anything time-dependence of the potential could further contribute to keeping seeds away from the galactic center. The external gravity and DF are calculated by Equation 1. Essentially, the difference between our “live” dynamics simulations and these post-processing calculations allows us to see how the time-dependence of the potential alters (in aggregate) the dynamics of sinking BH seeds.

To further see how the “lumpiness” of the potential alters the BH dynamics, we re-run our semi-analytic orbit integration in a “spherically-smoothed” version of the potential. In these calculations, we take the exact same spherically-averaged mass profile from the full simulation snapshot studied above,  $\rho(r) \equiv dM_{\text{enc}}(< r)/4\pi r^2 dr$  in narrow radial annuli  $dr$ , and then use this as the back-

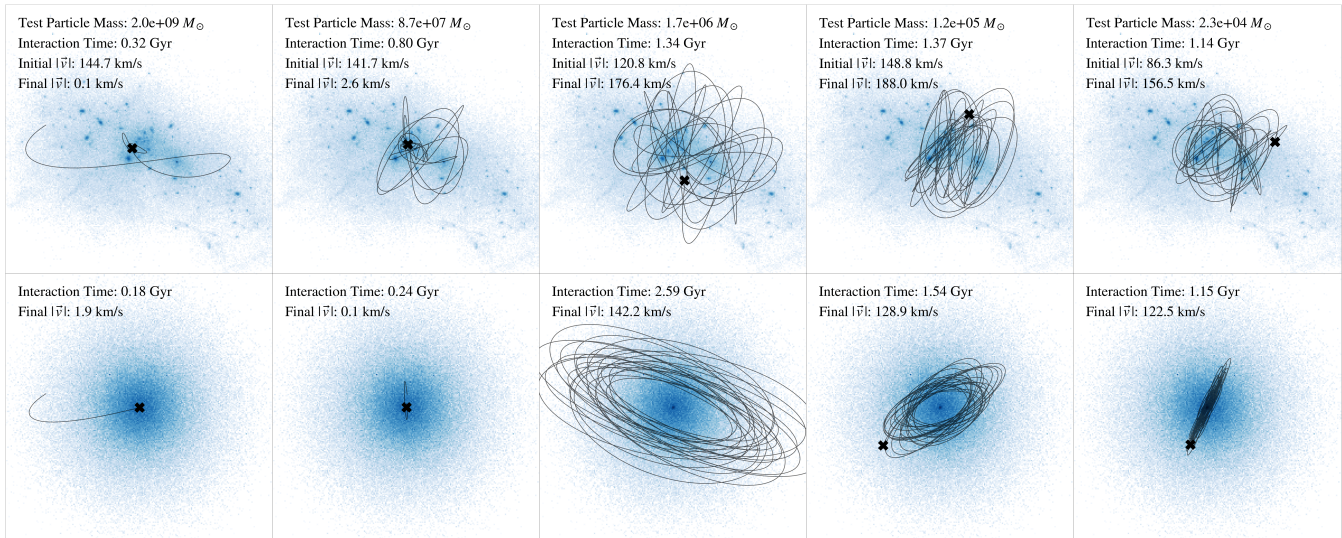


**Figure 3.** Sample orbits of several test particles (overlaid on top of the mass density distribution, shown in the blue colorscale) in the  $z = 7$  snapshot of “z5m12b” (**upper**) and its “spherically smoothed equivalent” (**lower**) where we take the identical enclosed mass profile  $M_{\text{enc}}(< r)$  and re-distribute the mass to be a perfectly-spherically-symmetric potential. The thin lines show the trajectories and the black cross shows the final positions of test particles. We find that in the high- $z$  galaxy, the most massive test particles do sink to the galactic center within a Hubble time at  $z = 7$  ( $\sim 1$  Gyr), while the low-mass seeds are simply experiencing chaotic orbits. In the smooth galaxy, the sinking behaviour is not very different for these five samples, yet for the massive seeds which are able to sink, their sinking time reduces drastically. This suggests that clumpy galactic backgrounds generally inhibit the sinking of massive seeds.

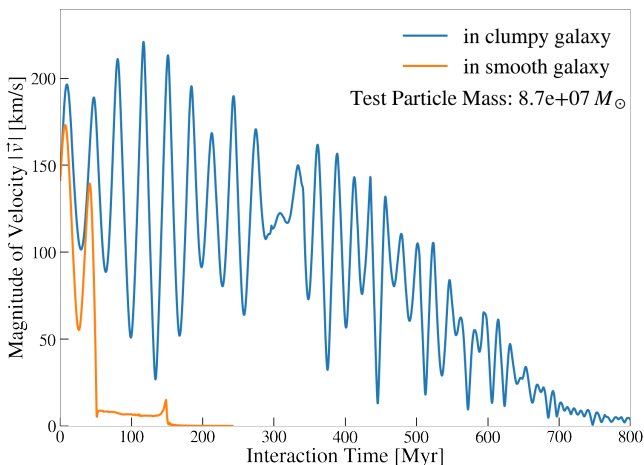


**Figure 4.** The evolution of the magnitude of the BH velocity as a function of interaction time for our integration of a  $8.7 \times 10^7 M_{\odot}$  test particle. We see that in both the clumpy and spherical smoothed galaxy, the velocity decays within 1 Gyr. But in the smooth galaxy the decay time is lower by about one order of magnitude than the clumpy case, suggesting again the clumpy and chaotic nature of early galaxies may drastically increase the sinking time of seed BHs.

ground potential for our orbit integration. So, by definition, this has the same spherically-averaged  $M_{\text{enc}}(< r)$  and circular velocity profile, but no substructure.

In Figure 3 we show several sample orbits for test particles of different masses in the  $z = 7.0$  snapshot of “z5m12b” overlaid on its mass density distribution. The orbits in the original snapshots are shown in the upper panel, while in the lower panel we show the trajectories integrated from the spherically smoothed version of this snapshot, with the same test-particle initial conditions. The thin lines show the trajectories and the black cross shows the final positions of test particles. The test particles follow chaotic orbits in the clumpy snapshot with no significant dynamical center (as we would

expect for a high- $z$  galaxy). It appears that for the most massive test particles  $M \gtrsim 10^8 M_{\odot}$ , their velocities significantly decrease within a Hubble time at  $z = 7$  ( $\sim 1$  Gyr), and their final positions lie within the very central region of the galaxy. But there is no significant sinking for low-mass test particles. In the smooth galaxy the particles behave similarly, yet it takes a shorter interaction time for the most massive test particles to sink. The velocity evolution of one particular test particle of  $8.7 \times 10^7 M_{\odot}$  is shown in Figure 4, and it is shown that the velocity decay timescale is about one order of magnitude shorter in the smooth galaxy compared to the clumpy galaxy. This suggests that the clumpy nature of early galaxies may increase the sinking time of seed BHs by an order of magnitude, by introducing chaotic dynamics to their orbits. In Figure 5 we show the initial and final positions of all test particles we integrate in this particular snapshot, and its spherically smoothed version. We also show their initial and final velocity magnitudes as a function of mass in the lower panel. In the clumpy galaxy, while the test particles are randomly distributed in the galaxy initially, those with  $M \gtrsim 10^8 M_{\odot}$  show clustering behaviour near the center after the integration, and their speeds decay to less than a few kilometers per second, indicating that they sink to the galactic center after the integration. The remaining low-mass particles remain scattered around, with no significant decay of their speeds. The smooth potential reduces the minimum sinking mass to  $\sim 10^7 M_{\odot}$ , when test particles are integrated over an order of the Hubble time at  $z = 7$ .

It appears that the clumpy nature of early galaxies may increase the “minimum sinking mass” by one order of magnitude. It is worth noting that the sinking massive particles in the clumpy galaxy also do not sink exactly to the same place near the center (as they do in the smooth galaxy). This implies that a clear definition of galactic center with resolution of a few hundred pc is still ambiguous for these galaxies, and has potentially major implications for the demographics of BH-BH mergers at high redshift.

In Figure 6 we show the initial and final magnitudes of galactocentric distance  $r$  and velocity  $v$  of all our test particles across different snapshots. The colored points show the final velocities and distances of test particles while the thin grey lines connect

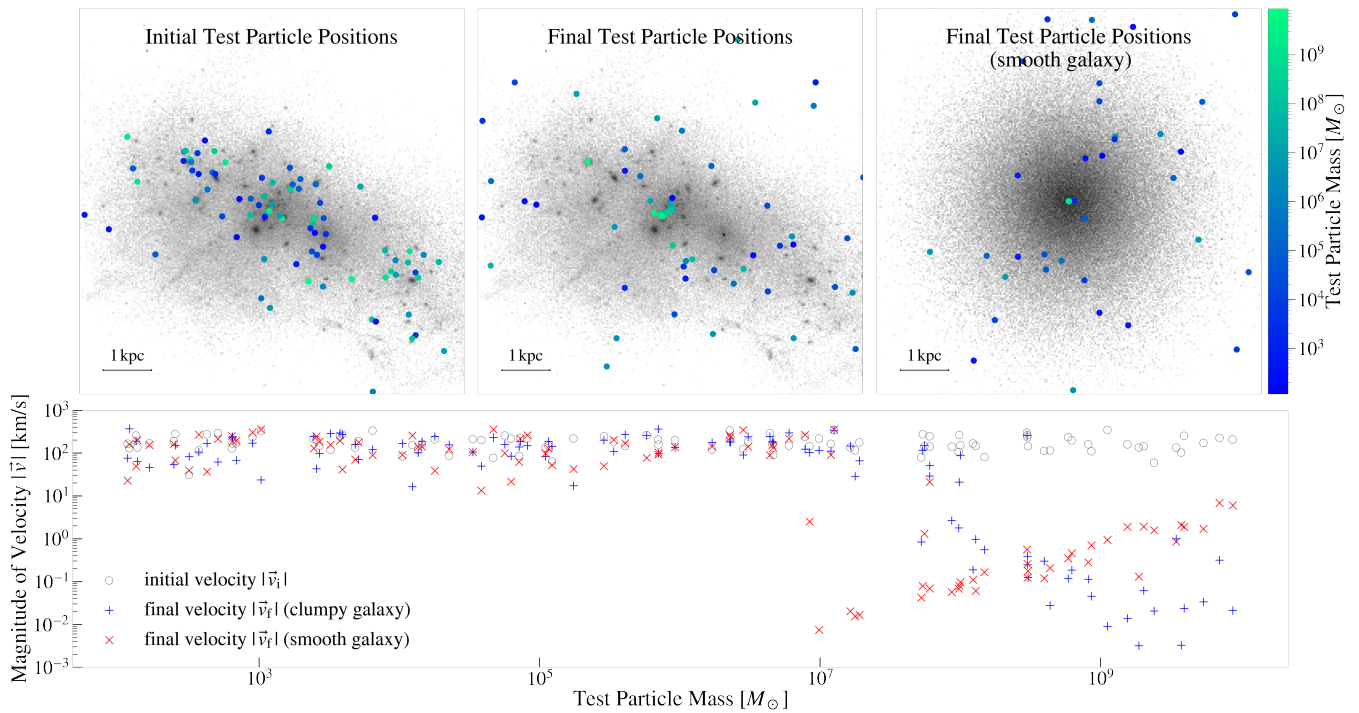


**Figure 5.** **Upper left:** The initial positions of test particles which we semi-analytically integrate, overlaid on the mass density distribution (grey) for “z5m12b” at redshift  $z = 7$ ; **Upper middle:** The final positions of these test particles. **Upper right:** The final positions of these test particles integrated in the spherically smoothed galaxy. The colors label the test particle masses. **Lower:** The magnitude of initial velocities and final velocities as a function of the BH mass. We see that for the clumpy galaxy, the high mass ( $M \gtrsim 10^8 M_\odot$ ) test particles sink to the galactic center after the integration, while the low mass particles remain randomly distributed. For the smooth galaxy the minimum mass for sinking reduces to  $M \gtrsim 10^7 M_\odot$ , about one order of magnitude lower. DF and sinking are negligible for the lower-mass seeds in both cases.

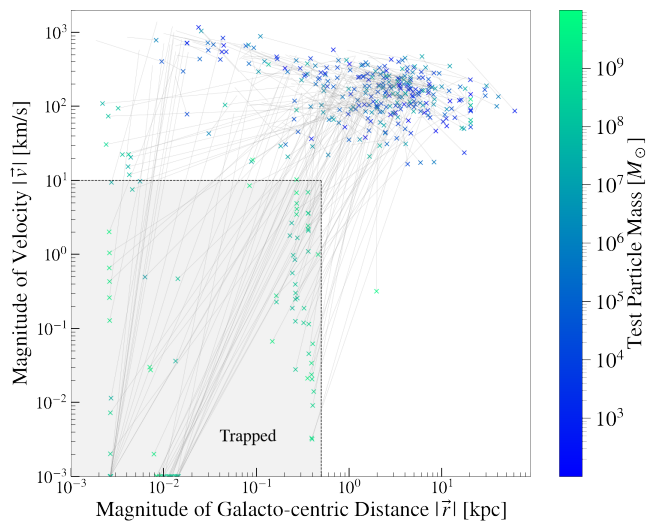


**Figure 6.** The initial and final magnitudes of velocities and galacto-centric distances of all our test particles across different snapshots. The colored points show the final velocities and distances (with any final velocities less than  $10^{-3}$  km/s interpreted as  $10^{-3}$  km/s for clarity). We define a BH particle as “trapped” as in Fig. 2. The thin grey line connects the final properties with initial properties of each particle. The colors label the mass of each particle. We can see that after our integration nearly all particles with masses  $\gtrsim 10^8 M_\odot$  sink to the galactic center (with a significant decline of velocity and distance), yet lower-mass particles are still randomly distributed.

their final values with initial values. We define the “sinking” region in phase space as in § 3.1. Since we are covering a larger mass range of test particles than what we did in direct simulations

for BH particles, some of the most massive particles do efficiently sink to the “trapped region” this time. Specifically, particles with  $M \gtrsim 10^8 M_\odot$  sink to the center region of the galaxy after the integration, regardless of their initial positions and velocities. For low-mass ( $M \lesssim 10^8 M_\odot$ ) particles, their final position and velocity distributions appear to be statistically similar to their initial configurations. This confirms the robustness of our results from direct simulations, in which all BH particles are less than  $10^8 M_\odot$  and are therefore not experiencing significant sinking. It is worth noting that the sinking criterion almost depends *entirely* on the particle mass, not on initial velocities/distances to galactic center.

## 4 DISCUSSION

From both direct simulations and semi-analytic post-processing calculations, we have found that seed BHs less massive than  $10^8 M_\odot$  generally cannot sink to galactic centers via DF in high- $z$  galaxies. To have at least one seed BH positioned in the galactic center so that it could accrete to  $\sim 10^9 M_\odot$  and provide a plausible origin for luminous high-redshift quasars, we discuss two categories of possible solutions.

### 4.1 Solution 1: Huge Numbers of Seeds, Forming Continuously

The first option is to use numbers as a trade off for efficiency: although one low-mass seed BH is not likely to sink and accrete, a huge number of low-mass seeds could possibly give an opportunity for a “lucky one” to sink and grow. Since the dynamics of BH particles and star particles are identically solved in our simulations (both as collisionless dynamics with external gravity), and the masses of star particles are around  $10^3 M_\odot$ , below the low-mass end where DF drag is significant, we can use the huge number of star particles

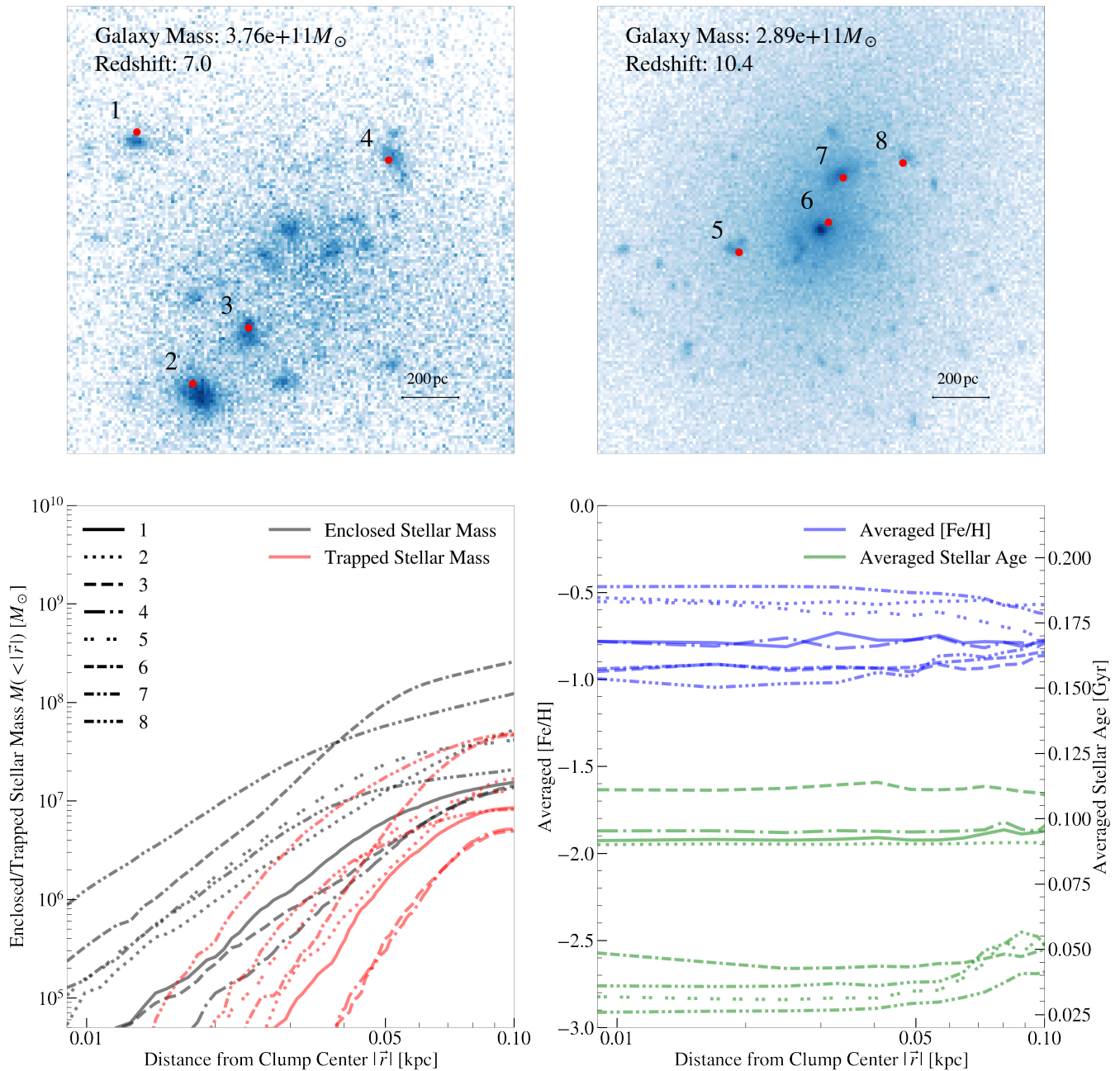


**Figure 7.** Behavior of low-mass test particles (e.g. stars) in individual high-density clumps (the “proto-bulge”) within our simulations. **Upper Left:** Mass density distribution of a  $z = 7$  galaxy with a total matter mass of  $3.8 \times 10^{11} M_{\odot}$ , where clumps 1-4 (the most massive bound sub-structures) are identified. **Upper Right:** Same for a  $z = 10.4$  galaxy with a total matter mass of  $2.9 \times 10^{11} M_{\odot}$ , where clumps 5-8 are identified. **Lower Left:** Enclosed stellar mass inside each clump as a function of clump-centric distance, and the “trapped” mass (defined as the mass which is bound with apocentric radii inside this radius, as opposed to e.g. stars on “plunging” or unbound orbits; see text). **Lower Right:** Mean stellar metallicity and age for star particles inside each clump. We see that only a few percent of the enclosed stellar particles could be trapped well inside ( $|\mathbf{r}| \lesssim 50$  pc) the clumps. The metallicity and age also indicate that most star particles (hence the clump) are formed recently, which leads to new problems for some scenarios for seed BH growth.

in our simulation as an ensemble of test particles to estimate the fraction of stars and therefore relics (ignoring processes like kicks) which can be trapped in local clustering structures (“clumps”). We apply such analysis to two particular snapshots, namely, “z5m12b” at  $z = 7.0$  and “z9m12a” at  $z = 10.4$ .

We are only interested in clumps broadly near the galactic center, hence we identify the four densest clumps within 1.6 kpc near the galactic center for each snapshot respectively, as shown in the upper panels of Figure 7. The center of the clumps are identified as the local density maxima, and their geometrical shapes are treated

as spherically-symmetric with radius 100 pc enclosing almost all of the clump mass, a fair approximation as shown in Figure 7.

The lower left panel of Figure 7 shows the enclosed stellar mass and trapped stellar mass as a function of radius around each clump. If a star particle at radius  $r$  has a maximum possible apocentric radius  $r_{\max}$  from the clump center (using the energy and angular momentum of each to evaluate its orbit, assuming the clump is static over its orbital timescale), we then say it is instantaneously enclosed within  $r$  and “trapped” within  $r_{\max}$ . The gravity potential is calculated assuming a static potential around each clump with spherical

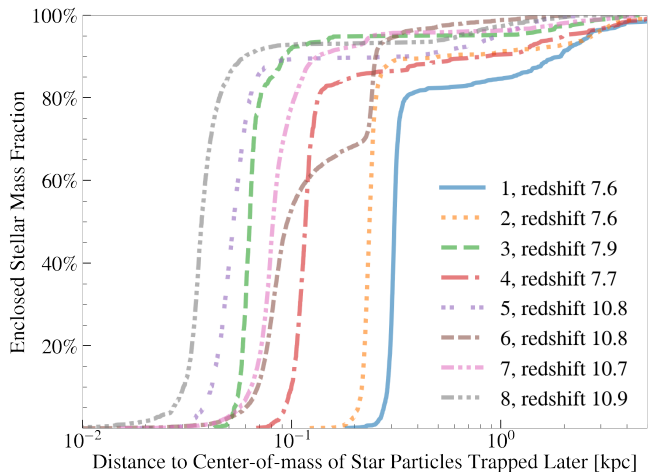


**Figure 8.** Distribution of “formation distances” for stars identified as enclosed in clumps in Fig. 7. We plot the cumulative distribution of distances between the center-of-mass of the main clump progenitor and the newly-formed star particle, at the time each star particle formed. We see that at least  $> 80 - 90\%$  of star particles in these clumps form “in situ,” at distances  $\ll 1$  kpc from the clump center. Only a small fraction are formed outside the clump and later captured. Of those, almost all form in the same galaxy at distances  $< 5$  kpc (as opposed to in satellites or different progenitor galaxies).

symmetry (the clumps themselves, by definition, do not have substantial substructure). We see that the stellar masses in each clump ( $M_{\text{enclosed}}(|\mathbf{r}| < 100\text{pc})$ ) range from  $10^7$  to  $10^8 M_{\odot}$ . The mass fractions of trapped stars differ for different clumps and around 30%-50% of stellar mass could be trapped in a  $\sim 0.1$  kpc radius of the clumps, yet this value decreases as we go deeper into the clump center, and the clumps could eventually trap only a few percent of enclosed star particles within  $\sim 50$  pc. For all clumps,  $\gtrsim 90\%$  of their mass is in stars (as opposed to gas or dark matter).

Some low-mass objects are trapped in the dense clumps that represent the proto-bulge of these galaxies. But do they actually “sink” or get trapped dynamically, or did they simply form in-situ? To track the formation history of these star particles, we show their distances to their center-of-mass at the particular redshift when most of them are just formed<sup>4</sup> in Figure 8. It turns out for almost all clumps,  $> 80 - 90\%$  of the star particles which we defined as “trapped” in these clumps are formed within  $\ll 1$  kpc from the clump-progenitor center-of-mass, which means most trapped star particles are formed in-situ. The only seemingly exception is clump 6, where at first glance it appears that only about  $\sim 70\%$  of the trapped star particles are in situ particles, but a detailed analysis shows that the remaining particles are actually formed in another clump which merges with clump 6, which does not challenge the conclusion (though it does relate to the hypothesis discussed in § 4.2). Taken together, this means that while it is possible in principle for “lucky” low-mass objects to be “trapped,” it is quite rare: comparing the total stellar mass of the galaxy to the mass of stars which form ex-situ and are trapped near clump centers yields a probability of about  $\sim 10^{-5} - 10^{-3}$  (depending on how generously we define “trapped”) for a low-mass seed formed randomly in the galaxy to migrate to being “trapped” in the central  $< 100$  pc of a clump by  $z \sim 7$ .

Even if this occurs, the metallicity of the star particles which undergo this processes may create new problems for seed models. While the first Pop III stars or “direct collapse primordial clouds,”

<sup>4</sup> The simulations we use generate one snapshot per 0.01 scalefactor, which is sufficient for this exercise.

which are candidates for forming massive seed BHs, could form very early at metallicities  $Z \ll 10^{-5} Z_{\odot}$ , the metallicity of star particles enclosed/trapped in clumps (even restricting to the “ex situ” stars) is generally much higher, and turns out to be the highest for the most massive clump, as shown in the lower right panel of Figure 7. This indicates that the trapped star particles in these clumps may not represent a fair sample of the ex-situ seed BH particles which are formed before the clumps themselves are formed. The earliest-forming stars are actually the *least* likely to be trapped in such clumps: they tend to form in mini-halos at much earlier times and therefore across many different progenitors and thus have to migrate in from the furthest distances, while the “ex situ but trapped” stars primarily still form in situ (*in the same galaxy*) just at distances of  $\sim 1$  kpc from the clump.

For all seed BHs, either in-situ or ex-situ, a related problem is related to the tension between the required clump masses and their ages. Seed BHs have a higher probability both to be initially trapped and to subsequently accrete gas rapidly in the most dense/massive clumps, but these clumps are preferentially formed later, hence providing less time for BHs to migrate and to accrete. The average age of star particles inside clumps, as shown in the lower right panel of Figure 7, is far less than the Hubble time at the redshift we examined, providing a strict constraint on duty cycle if seed BHs are indeed hyper-Eddington accreting to become SMBHs in these clumps. All these problems may lead to new constraints on SMBH formation channels.

## 4.2 Solution 2: Huge “Effective Masses” for Seeds

From the semi-analytic calculations in section 3.2 we have found that only seed particles as massive as  $\gtrsim 10^8 M_{\odot}$  can efficiently or reliably sink to galactic centers in a Hubble time. Such a large mass, however, is already a SMBH. On the other hand, our analysis in the previous section has shown that dense young star clusters as massive as  $10^7 - 10^8 M_{\odot}$  are present near the galactic center. In the previous section we also show that most trapped star particles within those clumps are already formed in situ. This suggests another possibility: while randomly formed seed BHs are generally not massive enough to decelerate individually via DF, their preferential formation in tightly bound structures with large “effective mass” is more realistic, as clusters could scatter with other components in the galaxy and sink effectively to the galactic center. Indeed, in X. Ma et al., in prep. we show that the most-massive clumps do merge efficiently as these simulations are run to lower redshift and form the “proto-bulge” of the galaxy.

There have been numerous papers arguing that runaway mergers in dense globular (star) clusters are a potential way to produce intermediate mass black holes (IMBHs, with typical masses  $10^2 - 10^5 M_{\odot}$ , see, e.g. Portegies Zwart & McMillan 2002; Gürkan et al. 2004; Shi et al. 2020; González et al. 2020), which naturally becomes a preferential way to embed massive BH seeds in dense clusters as described above. Such channels, however, suffer from other problems like large gravitational recoils that can remove the formed IMBHs from the cluster (e.g. Holley-Bockelmann et al. 2008). Observations have also put upper limits on IMBHs masses (e.g. Lützendorf et al. 2013, 2015; Kamann et al. 2016; Zocchi et al. 2017), which introduce additional constraints on this channel. It is also worth noting that, while globular clusters are usually assumed to be mainly pristine clusters that formed at very high redshift in mini-halos, hence define an “old” population for astrophysicists in the local universe, they are not so much older than the stars at  $z \gtrsim 7$ . In fact, the overwhelming majority of the clusters form *in-situ* in the galaxy as it evolves from in-situ gas, not from mini-halos merging in. This means that the metallicity and timing problems discussed in § 4.1 apply to this scenario, as well.

## 5 CONCLUSIONS

In this study, we explore high-resolution cosmological galaxy formation simulations to understand the dynamics of BH seeds at high- $z$  and their implications for SMBH formation and growth. Our simulations and semi-analytic DF calculations show that BH seeds cannot efficiently “sink” to galaxy centers and/or be retained at high redshifts unless they are extremely massive already,  $M > 10^8 M_\odot$ , i.e. already SMBHs. We show that this threshold is at least an order-of-magnitude higher than what one would expect in a spherically-symmetric smooth galaxy potential, as commonly adopted in analytic or older simulation calculations which could not resolve the complex, clumpy, time-dependent sub-structure of these galaxies. For smoother galaxies, this mass threshold reduces to  $10^7 M_\odot$ , which does not change the key conclusion.

We therefore join the growing number of recent studies by different groups which have reached similar conclusions (see e.g. Anglés-Alcázar et al. 2017b; Biernacki et al. 2017; Tremmel et al. 2018; Pfister et al. 2019; Bellovary et al. 2019b; Barausse et al. 2020; Boldrini et al. 2020). All of these studies, like ours, have concluded that this “sinking problem” for BH seeds may, in fact, be even more challenging than even other well-known challenges for explaining the formation and growth of the first SMBHs with masses  $\gg 10^9 M_\odot$  in galaxy centers at redshifts  $z > 7$ . Our contributions to extending this previous work include: (a) studying fully-cosmological simulations with higher resolution, a broader range of redshifts, a much broader spectrum of BH seed masses, and different (sometimes more detailed) explicit models for stellar feedback; (b) comparing direct cosmological simulations which only resolved N-body dynamics to semi-analytic post-processing models for DF, to verify that these conclusions are robust; and (c) extending our comparisons to the “test particle limit” by treating all stars as possible BH seeds.

Like these other studies, we qualitatively conclude that the chaotic, rapidly time-evolving, clumpy, bursty/dynamical nature of high-redshift galaxies, coupled to the very short Hubble times ( $\lesssim 1$  Gyr) make it nearly impossible for any lower-mass seeds to efficiently “migrate” from  $\gtrsim 1$  kpc scales to galaxy centers, and is far more likely to eject seeds than to retain them. Like these authors concluded, the clumpy, bursty nature of the ISM is crucial for these conclusions: so this can only be seen in simulations which resolve the cold phases of the ISM and explicitly model stellar feedback. It is also worth noting that for low-mass galaxies (the progenitors where, in most models, seeds are supposed to have formed), even at  $z \sim 0$ , clumpiness and burstiness are ubiquitous, and it is not simply a question of dynamical perturbations but even more basically of the fact that *dwarf and high-redshift galaxies do not have well-defined dynamical centers* to which anything *could* “sink.” This is true even for well-evolved galaxies such as the LMC today.

In fact, we show that even the extremely massive BHs ( $\gtrsim 10^8 M_\odot$  which do “sink” actually do not sink to the same location at sub-kpc scales, where their migration stalls. This has potentially profound implications for LISA detections of SMBH-SMBH mergers in high-redshift galaxies. Essentially, the “last parsec problem” so well-studied in the extremely dense, smooth, well-defined bulges of  $z = 0$  galaxies (where the Hubble time is long) becomes a “last kiloparsec problem” in these galaxies.

Solutions to the “sinking problem” for SMBH growth/formation generically fall into one of two categories which we discuss in detail. (1) Either seeds form “in situ” when the massive bulge finally forms and creates a deep central potential, or a huge number of seeds form so that even the infinitesimally small fraction which have just the right orbital parameters to be “captured” by this bulge can exist. In either case, the problem is that we show this deep central potential well does not form until quite

“late,” at redshift  $z \lesssim 9$ , from gas and stars which are already highly metal-enriched (metallicities  $\gtrsim 0.1 Z_\odot$ ). This would mean popular speculative BH seed formation channels like Pop III relics or “direct collapse” from hyper-massive quasi-stars could not provide the origin of the SMBHs. Moreover, the combination of the fact that this occurs late, and that the stellar IMF is “normal” at these metallicities, means that the “timescale” problem is much more serious: stellar-relic BHs must grow from  $\sim 10 M_\odot$  to  $\gg 10^9 M_\odot$  in  $\lesssim 200$  Myr – requiring sustained highly super-Eddington accretion. Alternatively (2) “seed” BHs must have enormous “effective” masses to form early and remain “trapped” and/or sink efficiently to the growing galaxy center. Of course, BHs “born” with  $M_{\text{BH}} \gg 10^7 M_\odot$  would solve this, but only by bypassing any stage that could be called a “seed” (moreover, no serious models involving standard-model physics can produce seeds of such large mass). However, models where seeds preferentially form tightly-bound in dense star cluster centers owing to physics not modeled here (for example, runaway stellar mergers in the center of dense, high- $z$  massive star clusters; see Shi et al. 2020) could (if the cluster is sufficiently dense) have an “effective” dynamical mass for our purposes of roughly the cluster itself, which could reach such large values. This suggests these regions may be promising sites for SMBH seed formation.

In future work, we will explore the role of BH accretion and feedback, and more explicitly consider models where BH seeds form in resolved star clusters, as well as a wider range of galaxy simulations. It is likely that *all* of the scenarios above require a sustained period of super-Eddington accretion, so we will also explore whether this requires seed BHs residing (or avoiding) certain regions within high- $z$  galaxies. We have also neglected models where non-standard model physics (e.g. dissipative dark matter, primordial BHs) allows for new formation channels and test-body dynamics. We will also explore new applications of our numerical dynamical friction approximator, in a variety of other interesting contexts (e.g. pairing of SMBHs in massive galaxy mergers at low redshifts).

## ACKNOWLEDGMENTS

We thank Zuyi Chen and Alessandro Lupi for useful discussions. Support for LM & PFH was provided by NSF Research Grants 1911233 & 20009234, NSF CAREER grant 1455342, NASA grants 80NSSC18K0562, HST-AR-15800.001-A. DAA acknowledges support by NSF grant AST-2009687 and by the Flatiron Institute, which is supported by the Simons Foundation. CAFG was supported by NSF through grants AST-1715216 and CAREER award AST-1652522; by NASA through grant 17-ATP17-0067; and by a Cottrell Scholar Award and a Scialog Award from the Research Corporation for Science Advancement. Numerical calculations were run on the Caltech compute cluster “Wheeler,” allocations FTA-Hopkins supported by the NSF and TACC, and NASA HEC SMD-16-7592.

## DATA AVAILABILITY

The data and source code supporting the plots within this article are available on reasonable request to the corresponding author.

## REFERENCES

- Alvarez M. A., Wise J. H., Abel T., 2009, *ApJ*, **701**, L133
- Anglés-Alcázar D., Davé R., Özel F., Oppenheimer B. D., 2014, *ApJ*, **782**, 84
- Anglés-Alcázar D., Davé R., Faucher-Giguère C.-A., Özel F., Hopkins P. F., 2017a, *MNRAS*, **464**, 2840
- Anglés-Alcázar D., Faucher-Giguère C.-A., Quataert E., Hopkins P. F., Feldmann R., Torrey P., Wetzel A., Kereš D., 2017b, *MNRAS*, **472**, L109
- Angles-Alcazar D., et al., 2020, arXiv e-prints, p. arXiv:2008.12303

- Bañados E., et al., 2018, *Nature*, **553**, 473
- Bañados E., et al., 2019, *ApJ*, **881**, L23
- Barausse E., Dvorkin I., Tremmel M., Volonteri M., Bonetti M., 2020, arXiv e-prints, p. [arXiv:2006.03065](https://arxiv.org/abs/2006.03065)
- Beifiori A., Courteau S., Corsini E. M., Zhu Y., 2012, *MNRAS*, **419**, 2497
- Bellovary J. M., Cleary C. E., Munshi F., Tremmel M., Christensen C. R., Brooks A., Quinn T. R., 2019a, *MNRAS*, **482**, 2913
- Bellovary J. M., Cleary C. E., Munshi F., Tremmel M., Christensen C. R., Brooks A., Quinn T. R., 2019b, *MNRAS*, **482**, 2913
- Biernacki P., Teyssier R., Bleuler A., 2017, *MNRAS*, **469**, 295
- Boldrini P., Mohayaee R., Silk J., 2020, *MNRAS*, **495**, L12
- Boylan-Kolchin M., Ma C.-P., Quataert E., 2008, *MNRAS*, **383**, 93
- Bromm V., Larson R. B., 2004, *ARA&A*, **42**, 79
- Bromm V., Loeb A., 2003, *ApJ*, **596**, 34
- Chandrasekhar S., 1943, *ApJ*, **97**, 255
- Colpi M., Callegari S., Dotti M., Kazantzidis S., Mayer L., 2007, in T. di Salvo, G. L. Israel, L. Piersant L. Burderi G. Matt A. Tornambe & M. T. Menna ed., American Institute of Physics Conference Series Vol. 924, The Multicolored Landscape of Compact Objects and Their Explosive Origins; AIP, Cefalu, Sicily (Italy). pp 705–714 ([arXiv:0706.1851](https://arxiv.org/abs/0706.1851)), doi:10.1063/1.2774931
- Corbett Moran C., Grudić M. Y., Hopkins P. F., 2018, arXiv e-prints, p. [arXiv:1803.06430](https://arxiv.org/abs/1803.06430)
- Davies M. B., Miller M. C., Bellovary J. M., 2011, *ApJ*, **740**, L42
- Decarli R., et al., 2018, *ApJ*, **854**, 97
- Decarli R., et al., 2019, *ApJ*, **880**, 157
- Devecchi B., Volonteri M., 2009, *ApJ*, **694**, 302
- Elmegreen D. M., Elmegreen B. G., Ravindranath S., Coe D. A., 2007, *ApJ*, **658**, 763
- Fan X., et al., 2001, *AJ*, **122**, 2833
- Fan X., et al., 2003, *AJ*, **125**, 1649
- Faucher-Giguère C.-A., 2018, *MNRAS*, **473**, 3717
- Faucher-Giguère C.-A., Lidz A., Zaldarriaga M., Hernquist L., 2009, *ApJ*, **703**, 1416
- Ferrarese L., Merritt D., 2000, *ApJ*, **539**, L9
- Gebhardt K., et al., 2000, *ApJ*, **539**, L13
- González E., Kremer K., Chatterjee S., Fragione G., Rodriguez C. L., Weatherford N. C., Ye C. S., Rasio F. A., 2020, arXiv e-prints, p. [arXiv:2012.10497](https://arxiv.org/abs/2012.10497)
- Graham A. W., Onken C. A., Athanassoula E., Combes F., 2011, *MNRAS*, **412**, 2211
- Grudić M. Y., Hopkins P. F., 2020, *MNRAS*, **495**, 4306
- Grudić M. Y., Hopkins P. F., Faucher-Giguère C.-A., Quataert E., Murray N., Kereš D., 2018, *MNRAS*, **475**, 3511
- Gürkan M. A., Freitag M., Rasio F. A., 2004, *ApJ*, **604**, 632
- Guszejnov D., Grudić M. Y., Hopkins P. F., Offner S. S. R., Faucher-Giguère C.-A., 2020, arXiv e-prints, p. [arXiv:2002.01421](https://arxiv.org/abs/2002.01421)
- Haiman Z., 2004, *ApJ*, **613**, 36
- Haiman Z., Loeb A., 2001, *ApJ*, **552**, 459
- Hirano S., Hosokawa T., Yoshida N., Umeda H., Omukai K., Chiaki G., Yorke H. W., 2014, *ApJ*, **781**, 60
- Hirano S., Hosokawa T., Yoshida N., Kuiper R., 2017, *Science*, **357**, 1375
- Holley-Bockelmann K., Gülltekin K., Shoemaker D., Yunes N., 2008, *ApJ*, **686**, 829
- Hopkins P. F., 2015, *MNRAS*, **450**, 53
- Hopkins P. F., Hernquist L., Cox T. J., Di Matteo T., Martini P., Robertson B., Springel V., 2005, *ApJ*, **630**, 705
- Hopkins P. F., Hernquist L., Cox T. J., Di Matteo T., Robertson B., Springel V., 2006, *ApJS*, **163**, 1
- Hopkins P. F., Hernquist L., Cox T. J., Kereš D., 2008, *ApJS*, **175**, 356
- Hopkins P. F., Narayanan D., Murray N., 2013, *MNRAS*, **432**, 2647
- Hopkins P. F., Keres D., Onorbe J., Faucher-Giguere C.-A., Quataert E., Murray N., Bullock J. S., 2014, *MNRAS*, **445**, 581
- Hopkins P. F., et al., 2018, *MNRAS*, **480**, 800
- Hosokawa T., Omukai K., Yorke H. W., 2012, *ApJ*, **756**, 93
- Hosokawa T., Yorke H. W., Inayoshi K., Omukai K., Yoshida N., 2013, *ApJ*, **778**, 178
- Hoyle F., Lyttleton R. A., 1939, *Proceedings of the Cambridge Philosophical Society*, **35**, 405
- Inayoshi K., Haiman Z., Ostriker J. P., 2016, *MNRAS*, **459**, 3738
- Inayoshi K., Li M., Haiman Z., 2018, *MNRAS*, **479**, 4017
- Inayoshi K., Visbal E., Haiman Z., 2019, arXiv e-prints, p. [arXiv:1911.05791](https://arxiv.org/abs/1911.05791)
- Johnson J. L., Bromm V., 2007, *MNRAS*, **374**, 1557
- Kallivayalil N., van der Marel R. P., Besla G., Anderson J., Alcock C., 2013, *ApJ*, **764**, 161
- Kamann S., et al., 2016, *A&A*, **588**, A149
- Katz H., Sijacki D., Haehnelt M. G., 2015, *MNRAS*, **451**, 2352
- Kawashima T., Ohsuga K., Mineshige S., Yoshida T., Heinzeller D., Matsumoto R., 2012, *ApJ*, **752**, 18
- Kim J.-h., Wise J. H., Abel T., Jo Y., Primack J. R., Hopkins P. F., 2019, *ApJ*, **887**, 120
- Kretschmer M., Teyssier R., 2020, *MNRAS*, **492**, 1385
- Lawrence A., et al., 2007, *MNRAS*, **379**, 1599
- Leitherer C., et al., 1999, *ApJS*, **123**, 3
- Li Y., et al., 2007, *ApJ*, **665**, 187
- Lupi A., Colpi M., Devecchi B., Galanti G., Volonteri M., 2014, *MNRAS*, **442**, 3616
- Lupi A., Haardt F., Dotti M., Fiacconi D., Mayer L., Madau P., 2016, *MNRAS*, **456**, 2993
- Lützgendorf N., et al., 2013, *A&A*, **552**, A49
- Lützgendorf N., Gebhardt K., Baumgardt H., Noyola E., Neumayer N., Kissler-Patig M., de Zeeuw T., 2015, *A&A*, **581**, A1
- Ma X., Hopkins P. F., Feldmann R., Torrey P., Faucher-Giguère C.-A., Kereš D., 2017, *MNRAS*, **466**, 4780
- Ma X., et al., 2018a, *MNRAS*, **477**, 219
- Ma X., et al., 2018b, *MNRAS*, **478**, 1694
- Ma X., et al., 2019, *MNRAS*, **487**, 1844
- Madau P., Rees M. J., 2001, *ApJ*, **551**, L27
- Madau P., Haardt F., Dotti M., 2014, *ApJ*, **784**, L38
- Meng X., Gnedin O. Y., 2020, *MNRAS*, **494**, 1263
- Mezcua M., Domínguez Sánchez H., 2020, *ApJ*, **898**, L30
- Milosavljević M., Couch S. M., Bromm V., 2009, *ApJ*, **696**, L146
- Morganson E., et al., 2012, *AJ*, **143**, 142
- Muratov A. L., Kereš D., Faucher-Giguère C.-A., Hopkins P. F., Quataert E., Murray N., 2015, *MNRAS*, **454**, 2691
- Novak M., et al., 2019, *ApJ*, **881**, 63
- Overzier R. A., Heckman T. M., Schiminovich D., Basu-Zych A., Gonçalves T., Martin D. C., Rich R. M., 2010, *ApJ*, **710**, 979
- Pacucci F., Volonteri M., Ferrara A., 2015, *MNRAS*, **452**, 1922
- Pezzulli E., Valiante R., Schneider R., 2016, *MNRAS*, **458**, 3047
- Pfister H., Volonteri M., Dubois Y., Dotti M., Colpi M., 2019, *MNRAS*, **486**, 101
- Planck Collaboration et al., 2020, *A&A*, **641**, A6
- Portegies Zwart S. F., McMillan S. L. W., 2002, *ApJ*, **576**, 899
- Portegies Zwart S. F., Baumgardt H., Hut P., Makino J., McMillan S. L. W., 2004, *Nature*, **428**, 724
- Regan J. A., Downes T. P., Volonteri M., Beckmann R., Lupi A., Trebitsch M., Dubois Y., 2019, *MNRAS*, **486**, 3892
- Reines A. E., Condon J. J., Darling J., Greene J. E., 2020, *ApJ*, **888**, 36
- Reinoso B., Schleicher D. R. G., Fellhauer M., Klessen R. S., Boekholt T. C. N., 2018, *A&A*, **614**, A14
- Ryu T., Tanaka T. L., Perna R., Haiman Z., 2016, *MNRAS*, **460**, 4122
- Shi Y., Grudić M. Y., Hopkins P. F., 2020, arXiv e-prints, p. [arXiv:2008.12290](https://arxiv.org/abs/2008.12290)
- Sijacki D., Vogelsberger M., Genel S., Springel V., Torrey P., Snyder G. F., Nelson D., Hernquist L., 2015, *MNRAS*, **452**, 575
- Sparre M., Hayward C. C., Feldmann R., Faucher-Giguère C.-A., Muratov A. L., Kereš D., Hopkins P. F., 2017, *MNRAS*, **466**, 88
- Springel V., Di Matteo T., Hernquist L., 2005, *MNRAS*, **361**, 776
- Swinbank A. M., et al., 2010, *MNRAS*, **405**, 234
- Takeo E., Inayoshi K., Ohsuga K., Takahashi H. R., Mineshige S., 2019, *MNRAS*, **488**, 2689
- Tremaine S., et al., 2002, *ApJ*, **574**, 740
- Tremmel M., Governato F., Volonteri M., Pontzen A., Quinn T. R., 2018, *ApJ*, **857**, L22
- Turner E. L., 1991, *AJ*, **101**, 5
- Velázquez J. A. F., et al., 2020, *MNRAS*, **494**, 1263
- Venemans B. P., et al., 2017, *ApJ*, **837**, 146
- Venemans B. P., Neeleman M., Walter F., Novak M., Decarli R., Hennawi J. F., Rix H.-W., 2019, *ApJ*, **874**, L30
- Volonteri M., 2012, *Science*, **337**, 544

- Wang F., Wang R., Fan X., Wu X.-B., Yang J., Neri R., Yue M., 2019, *ApJ*, **880**, 2
- Weisz D. R., Dolphin A. E., Skillman E. D., Holtzman J., Gilbert K. M., Dalcanton J. J., Williams B. F., 2014, *ApJ*, **789**, 147
- Whalen D., van Veelen B., O'Shea B. W., Norman M. L., 2008, *ApJ*, **682**, 49
- Willott C. J., et al., 2007, *AJ*, **134**, 2435
- Wu X.-B., et al., 2015, *Nature*, **518**, 512
- Zocchi A., Gieles M., Hénault-Brunet V., 2017, *MNRAS*, **468**, 4429
- Çatmabacak O., Feldmann R., Anglés-Alcázar D., Faucher-Giguère C.-A., Hopkins P. F., Kereš D., 2020, arXiv e-prints, p. [arXiv:2007.12185](https://arxiv.org/abs/2007.12185)
- van den Bosch F. C., Lewis G. F., Lake G., Stadel J., 1999, *ApJ*, **515**, 50